

Article

Design and Considerations: Microelectromechanical System (MEMS) Vibrating Ring Resonator Gyroscopes

Waqas Amin Gill , Ian Howard, Ilyas Mazhar and Kristoffer McKee 

Department of Mechanical Engineering, Curtin University, Perth, WA 6845, Australia;
i.howard@exchange.curtin.edu.au (I.H.); i.mazhar@curtin.edu.au (I.M.)

* Correspondence: waqasamin.gill@postgrad.curtin.edu.au (W.A.G.); k.mckee@curtin.edu.au (K.M.)

Abstract: Microelectromechanical system (MEMS) vibrating gyroscope design considerations are always intriguing due to their microscale mechanical, electrical, and material behavior. MEMS vibrating ring gyroscopes have become important inertial sensors in inertial measurement units (IMU) for navigation and sensing applications. The design of a MEMS vibrating ring gyroscope incorporates an oscillating ring structure as a proof mass, reflecting unique design challenges and possibilities. This paper presents a comprehensive design analysis of the MEMS vibrating ring gyroscope from the mechanical, electrical, and damping perspectives. The mechanical design of the MEMS vibrating ring gyroscope investigates the various frame designs of the vibrating ring structure, as well as the various beam structures, including rectangular and semicircular beam structures, which are analyzed using mathematical models and finite element analysis (FEA) simulations that provide an in-depth analysis of the stiffness and deflection of the vibrating structures. The electrical designs of the MEMS vibrating ring gyroscope are analyzed using various electrode configurations, electrostatic actuation, and capacitive detection mechanisms. The design analysis of various forms of damping, including viscous, structural, thermoelastic, and anchor damping, is discussed. The variety of design structures is investigated for MEMS vibrating ring gyroscopes' mechanical, electrical, and damping performance.

Keywords: MEMS; MEMS gyroscope; vibrating ring gyroscope; ring resonator; inertial sensors; IMU; MEMS design; mechanical design; electrical design; damping design



Citation: Gill, W.A.; Howard, I.; Mazhar, I.; McKee, K. Design and Considerations:

Microelectromechanical System (MEMS) Vibrating Ring Resonator Gyroscopes. *Designs* **2023**, *7*, 106. <https://doi.org/10.3390/designs7050106>

Academic Editor: Mateusz Dybkowski

Received: 8 August 2023

Revised: 6 September 2023

Accepted: 7 September 2023

Published: 11 September 2023



Copyright: © 2023 by the authors. Licensee MDPI, Basel, Switzerland. This article is an open access article distributed under the terms and conditions of the Creative Commons Attribution (CC BY) license (<https://creativecommons.org/licenses/by/4.0/>).

1. Introduction

In the advent of modern technology, where miniaturization, energy efficiency, and high-performance devices are paramount, microelectromechanical system (MEMS) devices made themselves integral to many advanced electronic systems and applications [1–5]. These microscale devices combine mechanical and electrical structures on the same platform to provide diverse applications, from healthcare to automotive. Among the variety of MEMS devices, MEMS vibrating ring gyroscopes contribute significantly to inertial sensing and navigation in various household and space applications [6–9]. Vibrating ring gyroscopes are quite popular in inertial navigation systems, where they detect precise rotational motion and accurately dictate the position for navigation. Additionally, using a MEMS vibrating ring gyroscope in military applications to control and target the missile on a specific location is another example of its stabilizing system importance in the sensor technology. Automotive applications for rollover stabilization with a MEMS vibrating ring gyroscope are key sensors to equip with the accelerometer.

The MEMS vibrating ring gyroscope's symmetric design structure provides numerous advantages over other vibrating gyroscopes. The symmetric design offers greater precision, resolution, mode matching at resonance frequencies, thermal stability, and gyroscope sensitivity [7,10–12].

Continuous design innovation contributed to the evolution of MEMS vibrating gyroscopes from the first developed single-ring resonator gyroscope with eight springs and anchor support to the new complex design structures. Single-ring resonators [13–15], multi-ring resonators [16,17], disk resonators [18–20], star-shaped resonators [21], cobweb-shaped resonators [22,23], cylinder-shaped resonators [24–26], etc., are some of the possible geometrical classifications for ring resonators. These design variations have been investigated to achieve optimal gyroscope performance [27].

The design's mechanical, electrical, and damping properties are crucial to the operation of the MEMS vibrating gyroscope. The mechanical integrity ensures the design's reliability under inconsistent conditions without compromising the gyroscope's sensitivity [13,28,29]. The electrical design components translate and provide continuous actuation to the motion of vibrating mechanical systems, as well as detect the motion and convert it into electrical signals for the operation of the gyroscope [30]. The placement of the electrodes whether outside or inside of the ring structure plays a pivotal role in the design and performance of the vibrating ring gyroscope.

The damping design analysis is crucial for controlling the vibrational energy, as it provides a system that can withstand severe environments and vibrate without causing damage. There are various damping mechanisms like viscous, structural, thermoelastic, and anchor damping mechanisms that affect the overall performance of the gyroscope. Material selection is another important factor that describes the geometric orientation and alters Young's modulus in different directions. The alteration in the mechanical properties of the material brings a significant mode mismatch between the driving and sensing resonance frequencies. However, silicon is the most popular choice of materials for fabricating MEMS vibrating gyroscopes.

However, many anomalies are still present regarding the conceptualization to the functionalization of the MEMS vibrating ring gyroscopes. For example, microfabrication processes while fabricating complex microstructures also introduce imperfections in the structures that affect the overall performance of the gyroscope [8,31]. Material selection, damping parameters, and mechanical and electrical design setups are just a few considerations that must be investigated before developing the MEMS vibrating ring gyroscopes [13,32].

This paper emphasizes and discusses mainly the MEMS vibrating ring gyroscope. The design considerations are from the perspective of mechanical, electrical, damping, material selection, and microfabrication processes for the vibrating ring gyroscope. The fundamentals of mechanical design, including the dynamic study of beam structures and different design frames, are mainly discussed and investigated. In the electrical design, the setup of the electrodes, the basics of electrostatic actuation and detection mechanisms, and fundamental equations are discussed. The damping section briefly discusses viscous, structural, thermoelastic, and anchor damping mechanisms for the MEMS vibrating ring gyroscope. Further, the selection of materials and their geometrical orientations on the gyroscope's performance and the microfabrication processes' complexities on the gyroscope performance are discussed in the following sections.

2. Mechanical Design

There are numerous mechanical vibrating structures presented for MEMS vibrating gyroscopes [33]. Four common types of MEMS vibrating gyroscopes were discussed in detail [27]. This paper aims to provide readers with a comprehension of the mechanical and electrical design fundamentals of the MEMS vibrating ring gyroscope. MEMS vibrating gyroscopes have a highly sensitive ring structure. The symmetric design of the vibratory ring gyroscope eliminates the cross-axis sensitivity, which is a major issue for other design structures. Additionally, the mechanical design provides temperature stability and enhanced shock resistance for harsh environments.

In Figure 1, the basic design structure of the MEMS vibrating ring gyroscope is depicted schematically. The ring structure acts as the system's proof mass; beam support structures

typically support the ring mass structure, and a centrally placed anchor holds up the entire vibrating structure. Several electrodes are positioned around the ring structure for driving, sensing, and tuning purposes. Figure 1 depicts the rectangular beams attached to the outer ring function as the system’s proof mass.

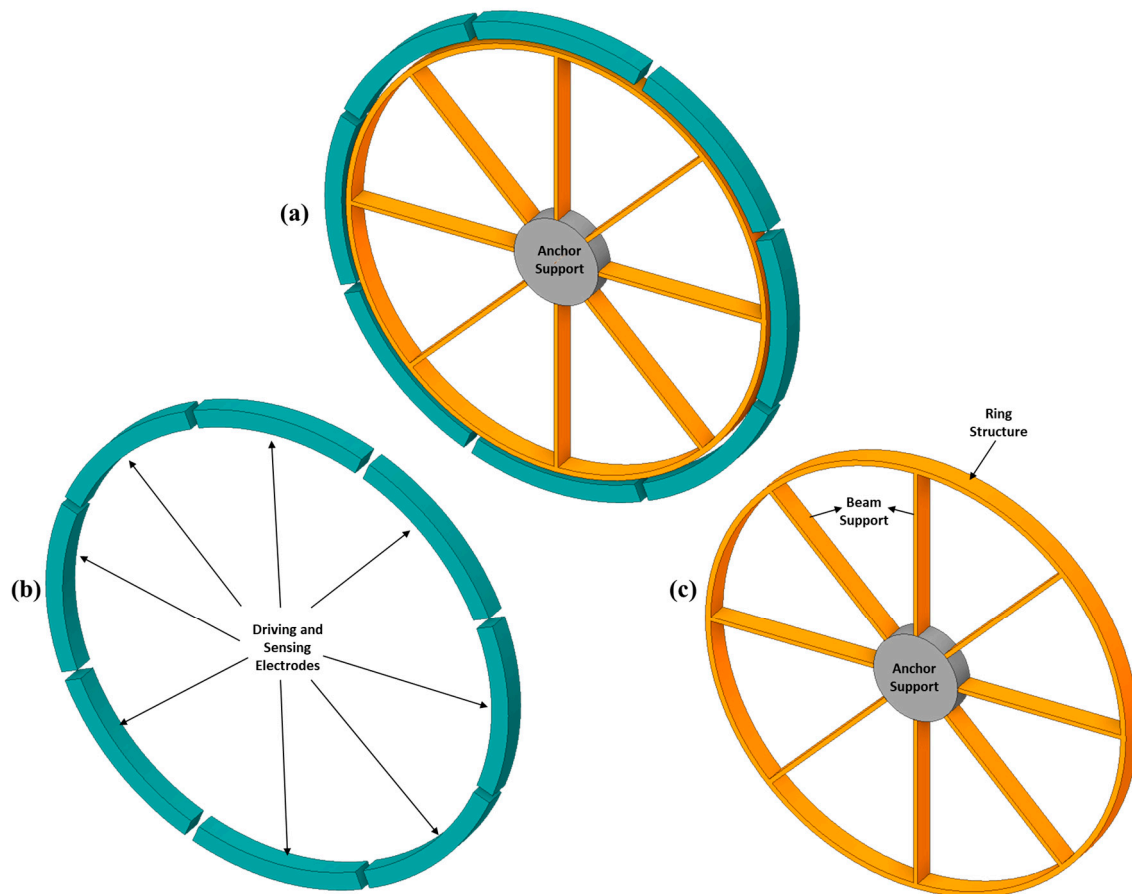


Figure 1. A schematic view of a simple vibrating ring gyroscope. (a) Gyroscope with electrodes. (b) Electrodes only. (c) Vibrating ring, beam support, and anchor support.

2.1. Dynamic Design System

The typical MEMS vibrating ring gyroscope design consists of the driving and sensing suspension systems. The driving suspension system has a set of driving electrodes, whereas the sensing suspension system has a set of sensing electrodes. The respective structure is positioned on top of the substrate. The driving and sensing electrodes are positioned at an angle of 45 degrees. Typically, the vibrating ring gyroscope has many mode shapes and can be represented by n modes. Elliptical mode shapes of vibrating rings are mostly considered for the ring gyroscope driving and sensing operation due to their identical shapes and minimum mode mismatching frequencies. The driving oscillation elliptical shape appears on the 45-degree node of the ring when the device is subjected to Z-axis rotation. The sensing electrodes detect the change in displacement and transmit the signal to the system in order to realign its position to its initial state. Figure 2 depicts the vibrating ring design structure’s schematic diagram.

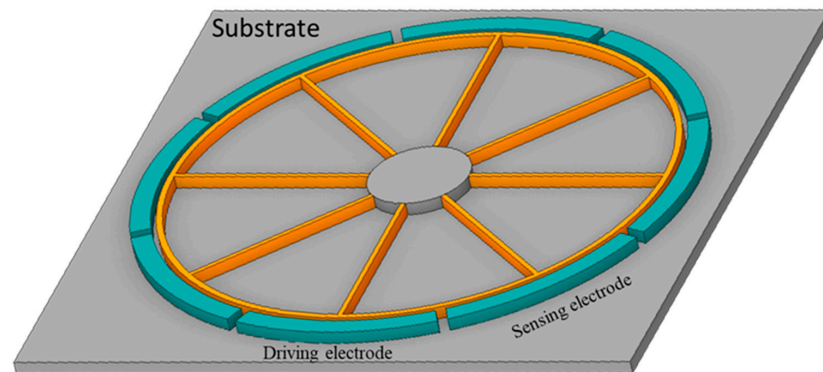


Figure 2. A schematic view of a simple vibrating ring gyroscope patterned on the substrate.

2.2. Beam Structures

Microelectromechanical system (MEMS) gyroscopes play a pivotal role as essential inertial sensors in a wide range of applications, encompassing navigation systems, mobile devices, digital cameras, gaming peripherals, and numerous other domains. The beam structures of these sensors consist of essential components. The design, selection of materials, and manufacturing processes employed in constructing these beam structures are crucial factors that significantly impact the reliability and operational effectiveness of the gyroscope. The beam structures facilitate the oscillation of the gyroscope mass in two opposing directions: the driving direction and the external rotation detecting direction. The driving and sensing systems utilize the same gyroscope mass for their operation. In order to ensure proper functioning, it is necessary for the gyroscope proof mass to possess the ability to oscillate freely along two axes.

The proof mass should also be constrained in one vibrational mode while oscillating in the other direction. The dynamic gyroscopic suspension system’s design has significance in achieving these objectives, as it assumes the responsibility of suspending the proof mass above the substrate. Several elastic beam structures are frequently employed in MEMS vibrating gyroscopes, and a selection of these structures is provided below.

2.2.1. Rectangular Straight Beam

A rectangular straight beam refers to a beam with a rectangular cross-section that maintains a straight shape. The suspended gyroscope construction consists of a proof mass that is connected to micro elastic beams. These beams are microfabricated using the same structural layer as the suspension system used in MEMS vibrating gyroscopes. The compliance of these elastic beams occurs along the driving direction while they remain stiff in the other sensing direction in the absence of rotation. Rectangular-shaped beams are frequently used in the domain of MEMS vibrating gyroscopes for translational oscillation. The rectangular beam structures are integrated with other beam structures in order to provide structural support for intricate gyroscope designs. Figure 3 shows the typical rectangular straight beam.



Figure 3. A schematic diagram of a rectangular-shaped beam.

The length of the rectangular beam is denoted as L when it is suspended along the X -axis. The width of the beam, suspended along the Y -axis, is represented as w . The height of the beam along the Z -axis is shown as h . The equation for the deflection of a rectangular beam can be stated as follows [34].

$$\delta_r = \frac{F}{k} \tag{1}$$

where F is the force applied toward the beam, k is the stiffness constant, and δ_r is the deflection that occurs when the beam is exposed to the applied force. The equation can be written as

$$k = \frac{24 E MoI}{L^3} \tag{2}$$

where E is the Young modulus, MoI is the moment of inertia, and L is the length of the rectangular beam. The moment of inertia is expressed in the axis differently. If the force is applied along the X -axis, the MoI is mathematically expressed as

$$MoI_x = \frac{1}{12}hw^3 \tag{3}$$

$$MoI_z = \frac{1}{12}h^3w \tag{4}$$

We can write stiffness constants for the rectangular beams along the three axes.

$$k_x = E \frac{hw^3}{L^3} \tag{5}$$

$$k_y = E \frac{hw}{L} \tag{6}$$

$$k_z = E \frac{h^3w}{L^3} \tag{7}$$

In the same way, the rectangular beam experiences a shear force, and therefore it is needed to find the stiffness constant because of the shear force exposed to the rectangular beam. The deflection occurs due to the applied force for the rectangular beam and is given as

$$\delta_r = \frac{3 F_a L}{5 whG} \tag{8}$$

where δ_r is the deflection due to the applied force, F_a is the applied force, G is the shear modulus $G = \frac{E}{2(1+\mu)}$, μ is the Poisson's ratio, L is the length of the beam, and $w \times h$ is the cross-sectional area of the rectangular beam. The stiffness constant due to the applied force can be written as

$$\frac{1}{k_r} = \frac{6 (1 + \mu)L}{5 whE} \tag{9}$$

2.2.2. Semicircular-Shaped Beam

There are many beam designs to consider for MEMS vibrating ring gyroscopes, with the semicircular-shaped beam being the most popular for vibrating ring gyroscopes. Figure 4 demonstrates the semicircular beam's schematic diagram.

The semicircular beams are subjected to applied force F_a and bending moments M_c . The stiffness constant k_t for semicircular beams is the sum of the stiffness constant k_t due to the applied force and stiffness constant due to bending moment k_b . The schematic view of the semicircular beam under applied force and bending moment is shown in Figure 5.

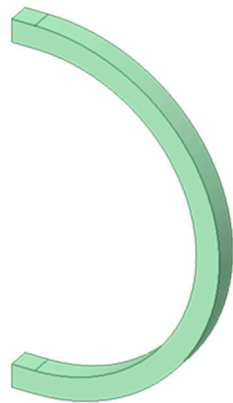


Figure 4. A schematic diagram of a semicircular-shaped beam structure.

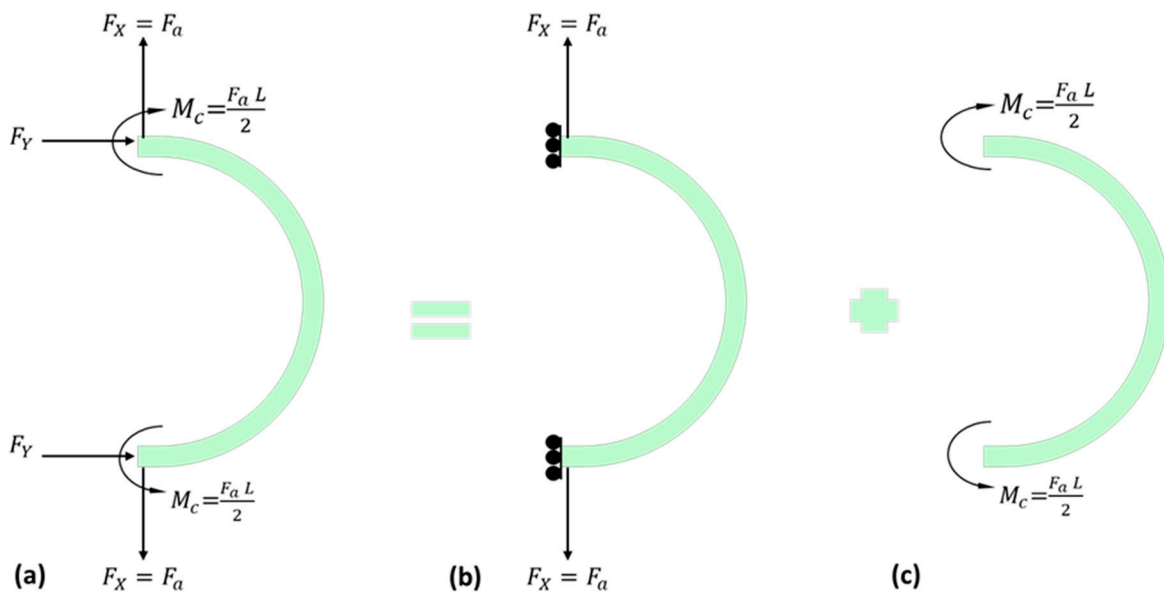


Figure 5. A schematic illustration of a semicircular beam subjected to (a) experienced forces and moments (b) applied force and (c) bending moments.

When a semicircular beam is subjected to applied force or external rotation, it experiences bending moment and normal forces; the stiffness constant for the semicircular beam can be calculated using the strain energy equation [35].

$$U_s = \int \frac{1}{2} \sigma \epsilon dV \tag{10}$$

where σ is the stress, ϵ is the strain, and U_s is the strain energy under applied force. The same equation can be written as

$$U_s = \int \frac{1}{2} \frac{\sigma^2}{E} dV \tag{11}$$

$$U_s = \int \frac{1}{2} E \epsilon^2 dV \tag{12}$$

$$\epsilon = \frac{My}{EI} \tag{13}$$

$$U_s = \int \frac{1}{2} \left(\frac{M^2 y^2}{EI^2} \right) dV \tag{14}$$

$$I_c = \int_{-h/2}^{h/2} y^2 w dy \tag{15}$$

$$U_s = \int_0^L \frac{1}{2} \frac{M^2}{EI_c} dx \tag{16}$$

where I_c is the moment of inertia, y is the distance from the neutral axis, w is the width of the beam, h is the height of the beam, M is the bending moment, E is the Young’s modulus of the material, and dx is the differential length of the beam.

The deflection of the semicircular beam can be described as

$$\delta_c = \frac{\partial U_s}{\partial F_a} \tag{17}$$

$$\delta_c = \frac{\partial}{\partial F_a} \int_0^L \frac{1}{2} \frac{M^2}{EI_c} dx \tag{18}$$

The length “ L ” of the semicircular beam can be described as

$$L = 2 \int_0^{\pi/2} r d\theta \tag{19}$$

where r is the defined radius of the semicircular beam, and θ is the angle in the semicircular beam. Only half of the semicircular beam will be considered because of the symmetrical structure design of the semicircular beam. The schematic view is shown in Figure 6.

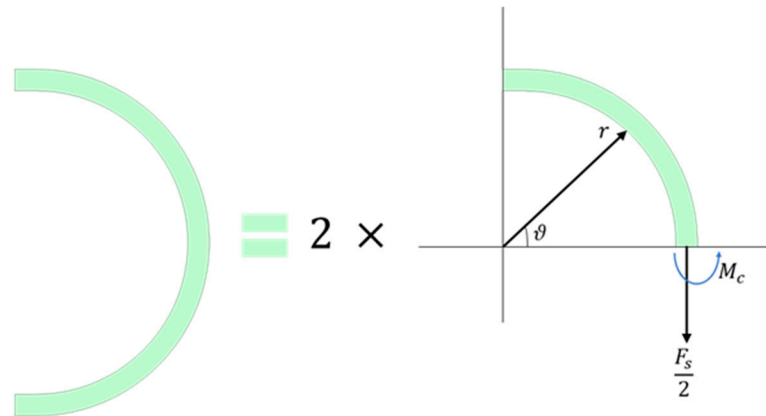


Figure 6. A schematic representation of a semicircular-shaped beam exposed to the applied force.

The deflection of the semicircular beam due to the applied force can be derived from the given equations shown below.

$$\delta_c = \frac{\partial U}{\partial F_a} = \frac{\partial}{\partial F_a} \left[2 \int_0^{\pi/2} \frac{M_c^2}{2EI_c} r d\theta \right] \tag{20}$$

$$\delta_c = \left[2 \int_0^{\pi/2} \frac{M_c}{EI_c} \frac{\partial M_c}{\partial F_a} r d\theta \right] \tag{21}$$

The semicircular-shaped beam is cut in half, and the bending moment M_c with the angle θ is given [36].

$$M_c = M_i - \frac{F_a r}{2} (1 - \cos\theta) \tag{22}$$

The half section of the semicircular-shaped beam experiences an imaginary bending moment due to the strain energy. The strain energy for the half section of the semicircular beam is shown below.

$$U_h = \int_0^{\pi/2} \frac{1}{2EI_c} M_c^2 r \, d\vartheta \tag{23}$$

$$U_h = \int_0^{\pi/2} \frac{1}{2EI_c} \left[M_i - \frac{F_a r}{2} (1 - \cos\vartheta) \right]^2 r \, d\vartheta \tag{24}$$

Since the above equation is for the half section of the semicircular beam, and if we have to find the strain energy of the complete semicircular beam U_c , the final equation becomes

$$U_c = 2U_h = 2 \int_0^{\pi/2} \frac{1}{2EI_c} \left[M_i - \frac{F_a r}{2} (1 - \cos\vartheta) \right]^2 r \, d\vartheta \tag{25}$$

The structure is symmetric, so $\vartheta = 0$, and $\frac{\partial U_h}{\partial M_i} = 0$.

$$0 = \frac{1}{EI_c} \int_0^{\pi/2} \left[M_i - \frac{F_a r}{2} (1 - \cos\vartheta) \right] r \, d\vartheta \tag{26}$$

$$\int_0^{\pi/2} \left[M_i - \frac{F_a r}{2} (1 - \cos\vartheta) \right] r \, d\vartheta = 0 \tag{27}$$

$$M_i = \frac{F_a r}{2} - \frac{F_a r}{\pi} \tag{28}$$

Equation (28) is substituted into Equation (22):

$$M_c = \frac{F_a r \cos\vartheta}{2} - \frac{F_a r}{\pi} \tag{29}$$

The partial derivative is taken with respect to the applied force F_a .

$$\frac{\partial M_c}{\partial F_a} = \frac{r}{2} \cos\vartheta - \frac{r}{\pi} \tag{30}$$

Equations (29) and (30) are substituted into Equation (21).

$$\delta_c = \frac{2}{EI_c} \int_0^{\pi/2} \left[\frac{F_a r \cos\vartheta}{2} - \frac{F_a r}{\pi} \right] \times \left[\frac{r}{2} \cos\vartheta - \frac{r}{\pi} \right] r \, d\vartheta \tag{31}$$

$$\delta_c = \frac{2F_a r^3}{EI_c} \int_0^{\pi/2} \left[\frac{\cos\vartheta}{2} - \frac{1}{\pi} \right] \times \left[\frac{\cos\vartheta}{2} - \frac{1}{\pi} \right] d\vartheta \tag{32}$$

$$\delta_c = \frac{2F_a r^3}{EI_c} \int_0^{\pi/2} \left[\frac{\cos\vartheta}{2} - \frac{1}{\pi} \right]^2 d\vartheta \tag{33}$$

The stiffness constant due to the applied and reaction forces of the semicircular-shaped beam can be expressed as Equation (34).

$$\frac{1}{k_c} = \frac{2r^3}{EI_c} \int_0^{\pi/2} \left[\frac{\cos\vartheta}{2} - \frac{1}{\pi} \right]^2 d\vartheta \tag{34}$$

The semicircular beam deflection due to the bending moments referred to in Figure 5c is investigated by using the strain energy equation method, as shown below.

$$U_c = \frac{1}{E} \int_0^{\pi/2} \frac{M_c^2}{I_c} r \, d\vartheta \tag{35}$$

$$U_c = \frac{\pi}{2} \times \frac{M_c^2 r}{EI_c} \tag{36}$$

As we know, the energy is equal to the work done on the system; therefore, we can write $E = \frac{1}{2}F\delta$, substituting the energy equation into Equation (36).

$$\frac{1}{2}F_a\delta_b = \frac{\pi}{2} \times \frac{M_c^2 r}{EI_c} \tag{37}$$

Similarly, Figure 5c shows the bending moment value of $M_c = \frac{F_a L}{2}$ substituted into Equation (37). The final deflection equation for the bending moment is given as Equation (38).

$$\delta_b = \frac{\pi F_a L^2 r}{4EI_c} \tag{38}$$

The semicircular-shaped beam’s stiffness constant is caused due to bending moments, and it can be determined by using Equation (39).

$$\frac{1}{k_b} = \frac{\pi r L^2}{4EI_c} \tag{39}$$

2.2.3. Semicircular Support Spring Structure

Semicircular support springs are commonly used in MEMS vibrating ring gyroscopes as support beams. This beam’s design structure consists of a combination of a semicircular beam and two rectangular beams. In earlier sections, the deflection and stiffness constant equations were presented. Figure 7 demonstrates the semicircular beam’s fundamental design. Typically, one end of the beam is connected to the anchor support as a fixed support, and the other is attached to the resonating structure.

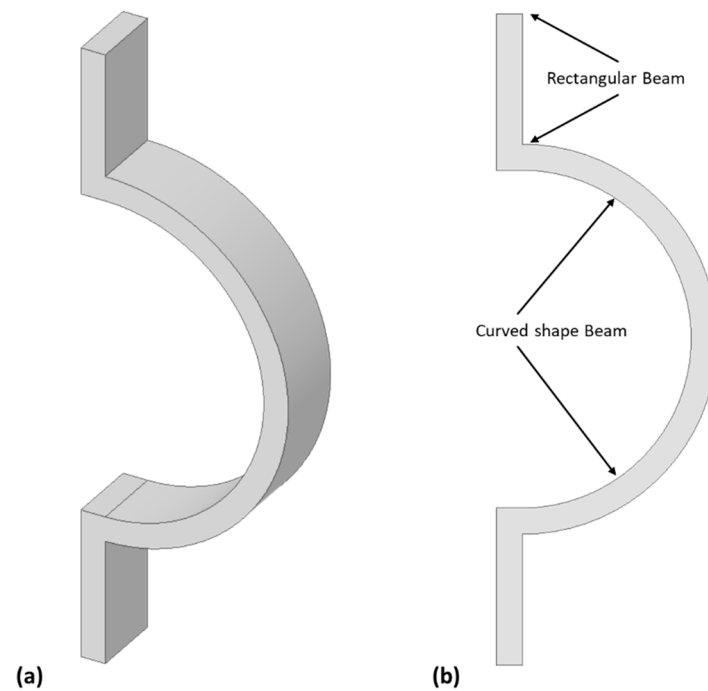


Figure 7. A schematic view of semicircular support spring: (a) 3D view (b) with its design description.

Applying the previously presented equations can determine the semicircular beam’s deflection. As the semicircular beam experiences applied forces, reaction forces, and bending moments, it undergoes deformation. To determine the deflections, we must use multiple equations presented in Table 1 for beam structures.

Table 1. Various beam design descriptions.

S. No.	Beam	Design	Deflections	Stiffness
1	Rectangular		$\delta_r = \frac{3}{5} \frac{F_a L}{whG}$	$\frac{1}{k_r} = \frac{6}{5} \frac{(1+\mu)L}{whE}$
2	Semicircular shape		$\delta_c + \delta_b = \frac{2F_a r^3}{EI_c} \int_0^{\frac{\pi}{2}} \left[\frac{\cos\theta}{2} - \frac{1}{\pi} \right]^2 d\theta + \frac{\pi F_a L^2 r}{4EI_c}$	$= \frac{2r^3}{EI_c} \int_0^{\frac{\pi}{2}} \left[\frac{\cos\theta}{2} - \frac{1}{\pi} \right]^2 d\theta + \frac{\pi r L^2}{4EI_c}$
3	Semicircular		$\delta_c + \delta_b + 2\delta_r = \frac{2F_a r^3}{EI_c} \int_0^{\frac{\pi}{2}} \left[\frac{\cos\theta}{2} - \frac{1}{\pi} \right]^2 d\theta + \frac{\pi F_a L^2 r}{4EI_c} + \frac{6}{5} \frac{F_a L}{whG}$	$\frac{1}{k_c} + \frac{1}{k_b} + \frac{1}{2k_r} = \frac{2r^3}{EI_c} \int_0^{\frac{\pi}{2}} \left[\frac{\cos\theta}{2} - \frac{1}{\pi} \right]^2 d\theta + \frac{\pi r L^2}{4EI_c} + \frac{3}{5} \frac{(1+\mu)L}{whE}$

2.2.4. Beam Structural Analysis

The analysis of semicircular beam deflection is conducted using Ansys 2023 R1. The study is conducted using the static structural module. The semicircular beam is composed of two rectangular beams and a semicircular-shaped beam. The semicircular beam used in the comparison experiments has a radius of 75 μm and a length of 60 μm. The heights of the beam vary between 30 μm and 60 μm. The semicircular beam is subjected to an applied force ranging from 100 μN to 1500 μN. The deflections of the beams are simulated, and analytical results are achieved by using the derived equations. The comparative results obtained from varying beam heights are presented in Figure 8.

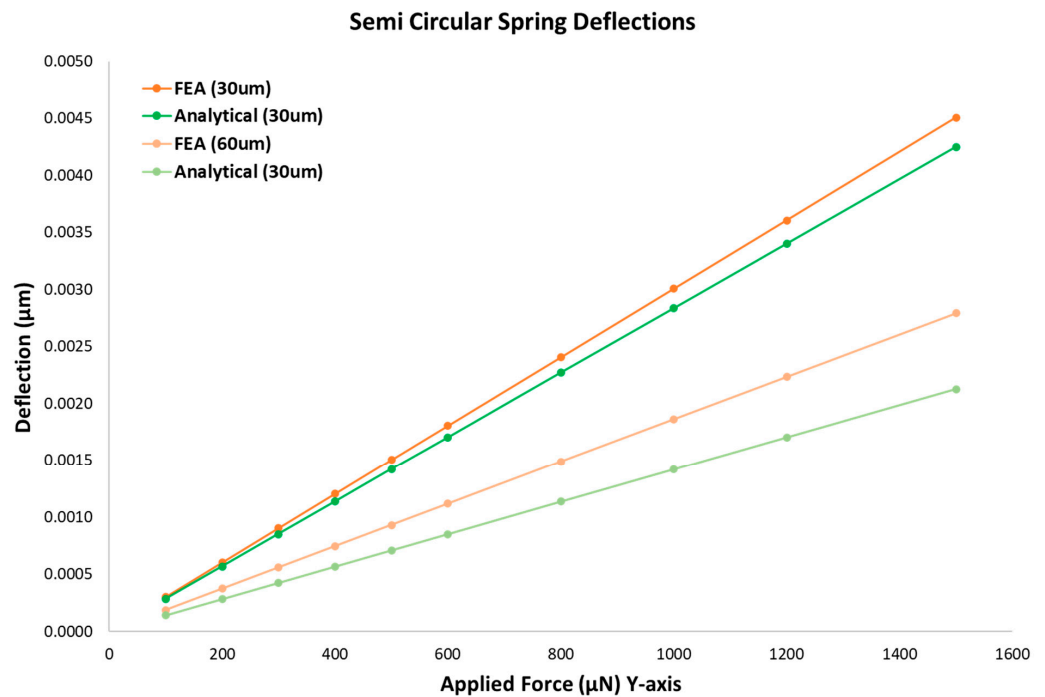


Figure 8. The semicircular beam’s deflection results in a comparison of finite element analysis (FEA) and analytical results.

The frequency analysis of the semicircular beam is examined using both Ansys 2023 R1 and analytical methods. The measured frequency observed in the simulation is 5.25 MHz, while the calculated natural frequency is determined to be 5.57 MHz. Table 2 displays the stiffness constant findings obtained from the modeled and analytical methods for the semicircular beam. The minimal percent errors for the frequency and the stiffness constant show the reliability of the derived analytical equations for the semicircular beam and the comparison of the results with Ansys 2023 R1. Figure 9 illustrates the modal frequency of the semicircular beam.

Table 2. Comparative design results for semicircular beam.

	Frequency (MHz)	Error	Stiffness Constant (kN/m)	Error
Ansys 2023 R1	5.25		353.6	
Analytical	5.57	5.74%	347.9	1.61%

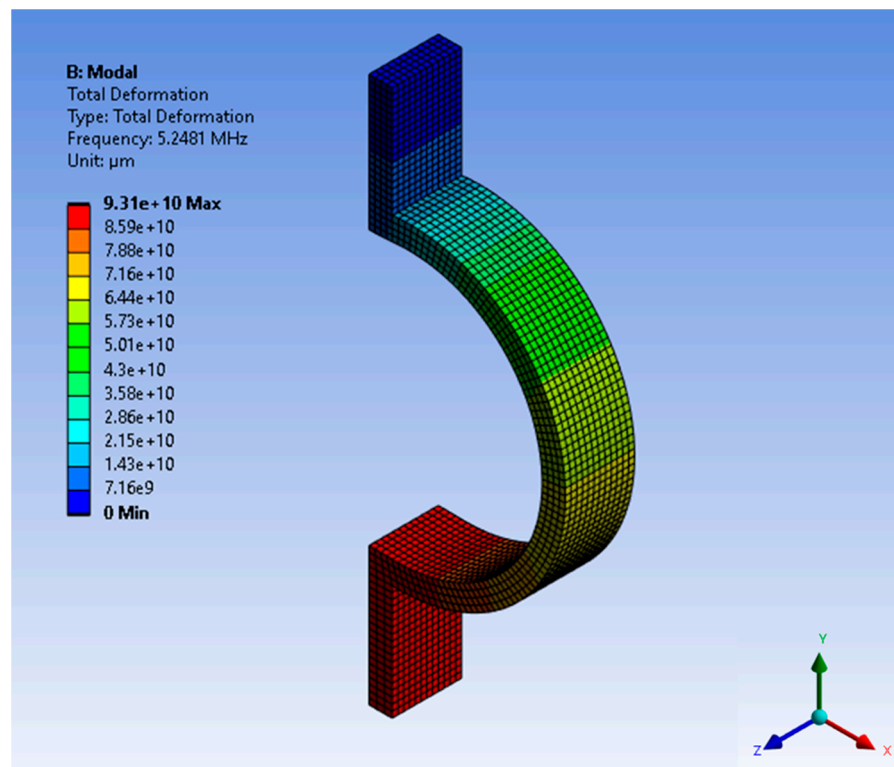


Figure 9. Modal frequency of the semicircular beam.

2.3. Design Frames for MEMS Vibrating Ring Gyroscopes

The frame structures of MEMS vibrating ring gyroscopes are crucial parameters for improving performance, reliability, and decoupling vibrational modes. The frame structures are mainly divided into two broad categories: internal ring structure and outer ring structure. Both of the design frames are discussed below.

2.3.1. Internal Ring Frame Design

In internal ring designs, the anchor support is placed outside the vibrating structure, and the ring structure is connected to the fixed anchor support pillar via flexible elastic beams [37]. By isolating the vibrating structure from any undesirable external vibrations, this internal ring design configuration has the potential to enhance the gyroscope’s performance. Internal ring structures are highly adaptable and durable, making them crucial inertial sensors for severe, harsh environments [10]. They are well-suited for use in spacecraft and other related applications that may be exposed to harsh environments due to their

resistance to unwanted vibrations. The schematic representation of the internal ring frame design is shown in Figure 10.

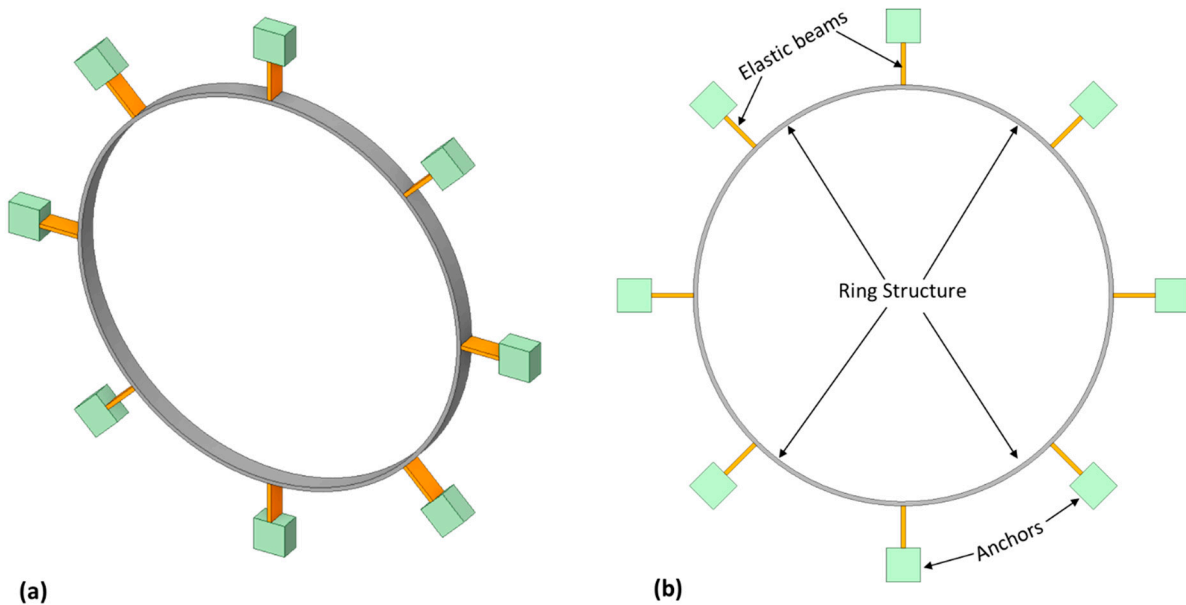


Figure 10. A schematic diagram of the inner ring frame design (a) in 3D view (b) with design description.

2.3.2. External Ring Frame Design

Incorporating an external ring frame is a common design technique utilized in designing and developing MEMS vibrating ring gyroscopes. The design of the external ring frame includes the placement of the support anchor and the elastic beam structure inside the ring structure. Significantly enhancing the overall sensitivity of the gyroscope, this design approach’s ability to accommodate a reasonably larger vibrating structure is a significant advantage. In contrast to the internal ring frame design, however, this particular design approach presents numerous challenges, particularly in its robustness in harsh environments. A schematic diagram of the external ring frame design is shown in Figure 11.

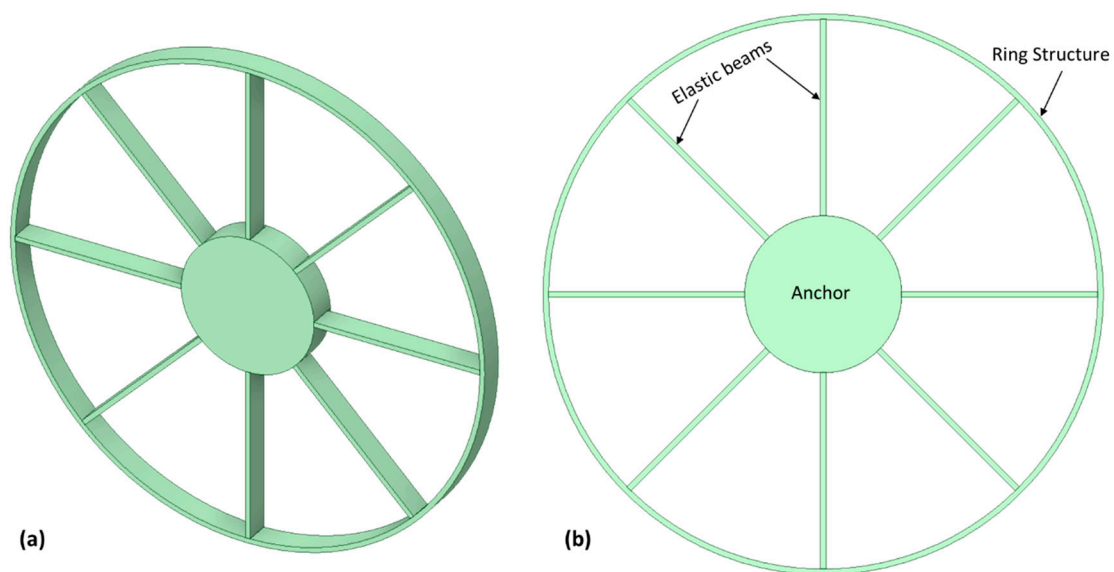


Figure 11. A schematic diagram of the external ring frame design (a) in 3D view (b) with design description.

Numerous designs of vibrating ring gyroscopes can benefit from the use of internal and external ring frame designs. The structures include single-ring gyroscopes, multi-ring gyroscopes, disk resonator gyroscopes, cylindrical shapes, shell forms, and star-shaped structures. The design of the external ring frame can accommodate all of these gyroscope structures. In contrast, the internal ring design of single-ring gyroscopes is quite advantageous. The internal area could be used to install additional tuning electrodes or to deploy and design a small inertial sensor in that space, such as an accelerometer or magnetometer.

2.3.3. FEM Modal Analysis

The FEM modal analysis is an essential computational analysis, especially when finding the vibration characteristics of mechanical structures like the MEMS vibrating ring gyroscope. This method provides a deep understanding of the behavior and modal frequencies of the vibrating ring gyroscope. The FEM modal analysis provides a clear picture of the vibrational modes and frequencies by breaking down the gyroscope structure into finite elements and resolving equations. The FEM modal analysis was conducted for both internal and external ring frame designs.

Internal Ring Frame Design: As illustrated in Figure 12, the internal ring frame design of the MEMS vibrating ring gyroscope is analyzed by its unique structural modification. The design constitutes eight semicircular beams, all of which are attached to the internal ring resonator. The whole vibrating structure is supported by externally placed anchors around the vibrating structure. This design strategy isolates the vibrating ring structure from external disturbances that could affect the gyroscope performance. The design specifications include a ring radius of $1000\ \mu\text{m}$, a radius of the semicircular beam of $200\ \mu\text{m}$, the thicknesses of the ring and beams of $10\ \mu\text{m}$, and a height of the structure of $30\ \mu\text{m}$. The modeled frequencies shown in Figure 13 for the internal ring design are $48,263\ \text{Hz}$ and $48,277\ \text{Hz}$ for mode 1 and mode 2, respectively.

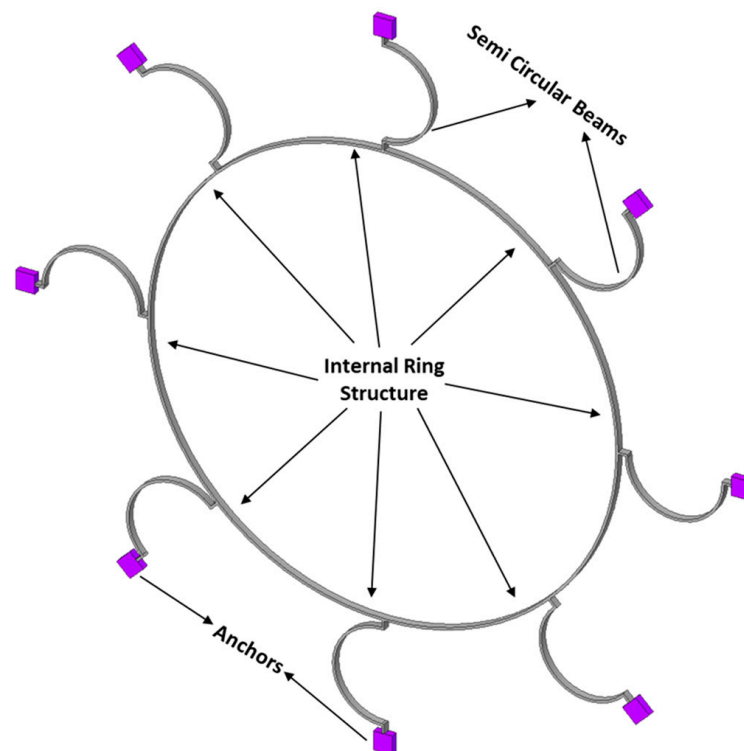


Figure 12. A schematic diagram of internal ring frame design with semicircular beams.

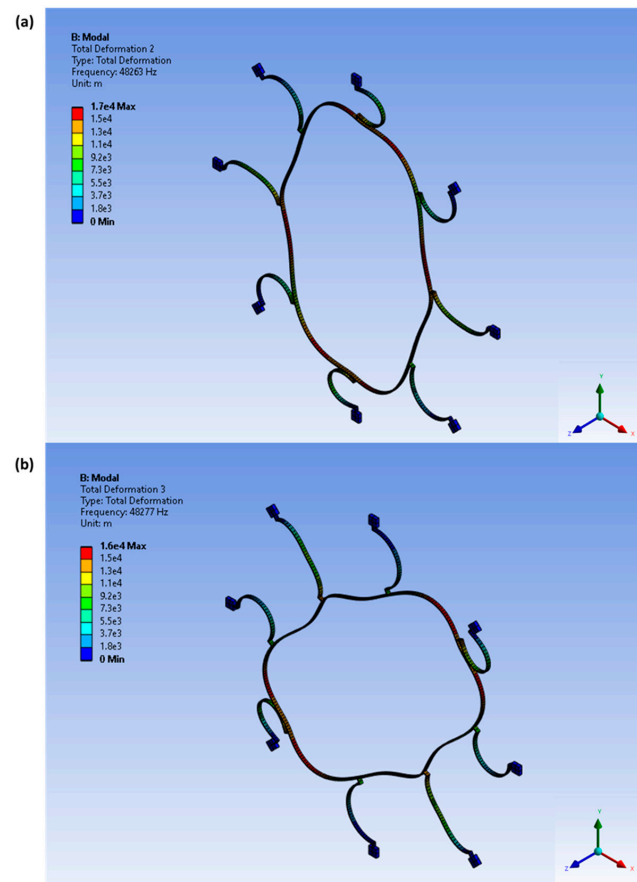


Figure 13. Modal frequencies of internal ring frame design gyroscope (a) Mode 1 (b) Mode 2.

External Ring Frame Design: On the other hand, the external ring frame design, as illustrated in Figure 14, presents a typical vibrating ring design approach [38]. This design also shows eight semicircular beams attached to the external ring resonator, and the whole vibrating structure is connected to the centrally placed circular anchor. The design specifications include a ring radius of 1000 μm , a semicircular beam radius of 200 μm , thicknesses of the ring and the beams of 10 μm , and the height of the structure of 30 μm . The recorded frequencies are shown in Figure 15, which are 40,241 Hz for mode 1 and 40,272 Hz for mode 2, respectively.

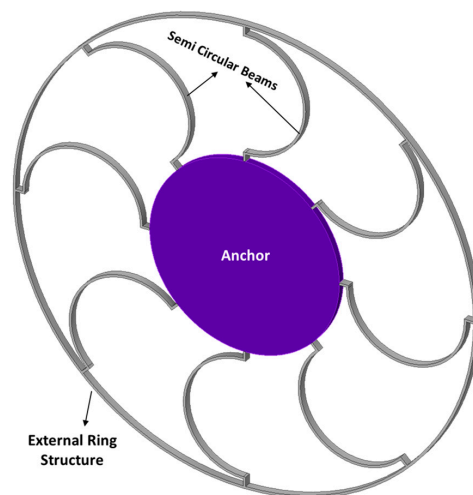


Figure 14. A schematic diagram of external ring frame design with semicircular beams.

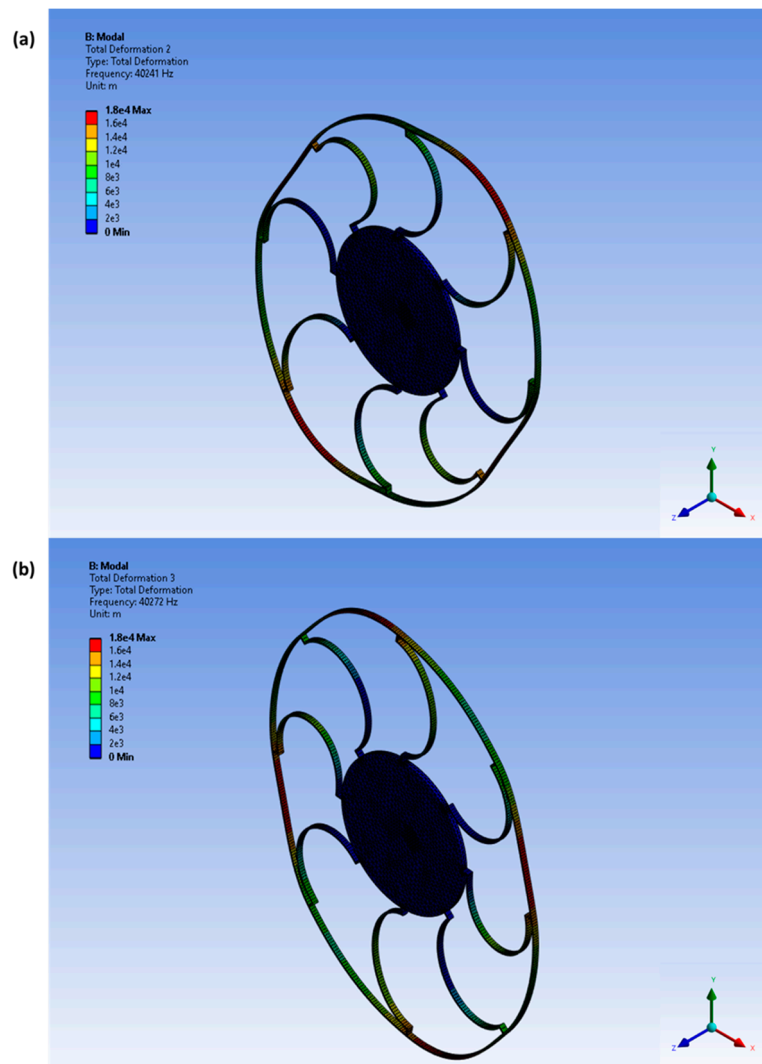


Figure 15. Modal frequencies of external ring frame design gyroscope (a) Mode 1 (b) Mode 2.

Both designs have the same design features, except the design geometry. The vibrating ring radius and radiuses for semicircular beams are the same for both designs. However, the internal ring frame design records elliptical mode shapes around 48 kHz, and the external ring frame design records elliptical mode shapes around 48 kHz. As can be seen in Table 3, the mode mismatches are recorded at 14 Hz and 31 Hz for internal and external ring frame designs, respectively. The results show that the internal ring frame design has better sensitivity and less split between the identical modes of vibrations, which makes the internal ring frame design more desirable than the external ring frame design for vibrating ring gyroscopes.

Table 3. Comparative design FEM modal analysis.

Frequency (Hz)	Internal Ring Design	External Ring Design	Ring Radius (μm)	Ring Thickness (μm)	Beam Radius
Mode 1	48,263 Hz	40,241 Hz	1000	10	200
Mode 2	48,277 Hz	40,272 Hz	1000	10	200
Mode Mismatch	14 Hz	31 Hz	1000	10	200

3. Electrical Design

MEMS vibrating ring gyroscopes are those MEMS devices that require a constant force to operate. In general, MEMS gyroscopes require an actuation mechanism for continuous oscillation and a detecting system when the gyroscope is subjected to external rotation. The MEMS vibrating ring gyroscope is typically operated using a variety of actuation and detecting techniques. The actuation mechanisms include piezoelectric, magnetic, electrostatic, and thermo-actuation, whereas the detecting mechanisms include piezoelectric, capacitive, optical, and magnetic.

The electrode setup is also very significant when developing a gyroscope design, as the designed electrodes provide actuation and detecting mechanisms. The electrode setup design for the MEMS vibrating ring gyroscope is discussed in detail below.

3.1. Electrode Setup

The vibrating ring structure is the most essential part of the MEMS vibrating ring gyroscope design. Multiple electrodes encompass the structure of the vibrating ring for driving and sensing purposes. The driving electrodes provide a continuous motion in two orthogonal axes. On the other hand, the sensing electrodes detect the change in displacement between the ring and the sensing electrode when the gyroscope is exposed to external rotation. There are many ways in which electrodes could be placed around the vibrating ring structure. Some of the common electrode placements in vibrating ring gyroscopes are discussed below.

3.1.1. Outside Placement

In this configuration, the electrodes are positioned outside of the vibrating ring structure, while the inner portion of the ring is sustained by flexible beams with a central anchor. This configuration offers numerous advantages, including simple design, efficient connection, simple fabrication, and reduced electronic complexity. However, this design configuration tends to increase device size, which could restrict its use in many electronic applications due to space constraints.

3.1.2. Inside Placement

In this design configuration, the electrodes are positioned within the vibrating ring structure, while the ring's exterior is covered and supported by flexible beams with an outer anchor. This design configuration accommodates a compact device area, making it suitable for miniaturized electronic devices. However, positioning electrodes within the ring structure complicates the design and requires intricate microfabrication processes.

3.1.3. Both Inside and Outside

In this design configuration, electrodes are positioned inside and outside the vibrating ring structure for optimal results. This type of design configuration effectively minimizes undesirable errors, such as geometrical imperfections caused by microfabrication tolerances, matches resonance frequencies, and eliminates other related errors. However, the complexity of the device's design, fabrication, and electronic circuitry is increased by this design configuration.

All three electrode setup designs are shown in Figure 16.

The design configuration of electrodes can be utilized for a variety of purposes. The advantage of the ring structure is the placement of numerous electrodes around the vibrating structure. Some of the primary functions of electrodes are listed below.

1. **Driving Electrode:** Driving electrodes apply a continuous electrostatic actuation force to the ring's structure, causing it to oscillate in the driving direction.
2. **Sensing Electrode:** These electrodes detect the change in displacement when the device is subjected to rotation via an electrostatic detection mechanism.
3. **Tuning Electrode:** This type of electrode adjusts the resonance frequency to achieve optimal results, thereby enhancing the ring gyroscope's sensitivity. The tuning elec-

- trodes used to be placed around the vibrating ring structure. These electrodes tune the frequency shift between the two operating resonance frequencies [39].
4. Quadrature Electrode: These electrodes mitigate the quadrature error that arises as a result of microfabrication or geometrical inaccuracies.

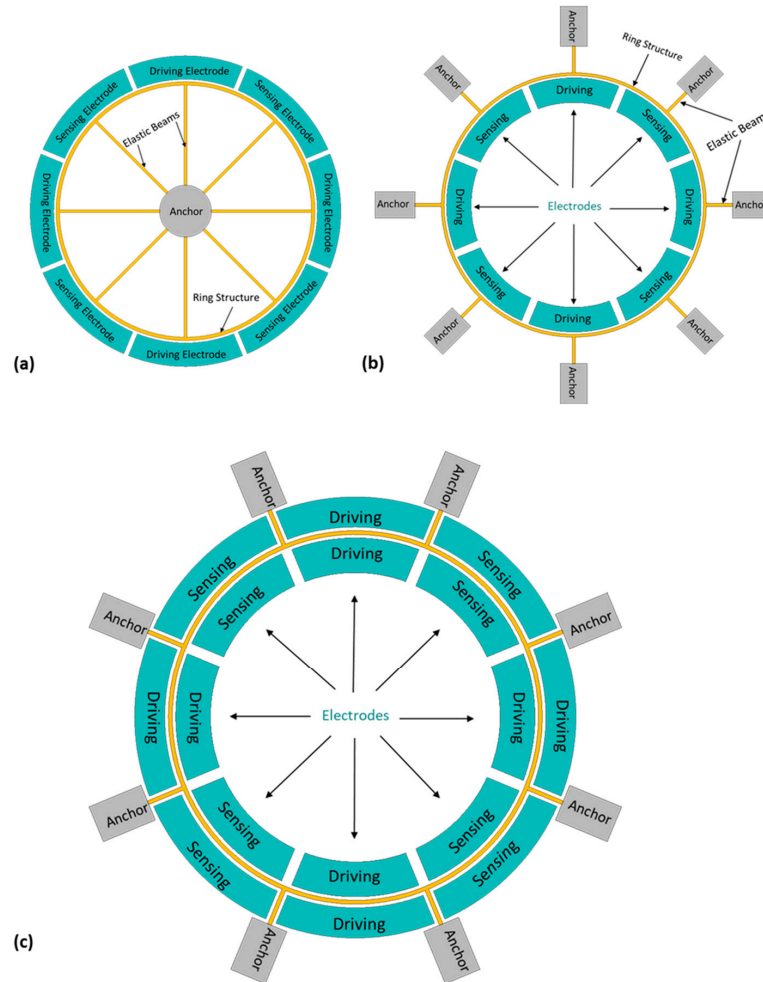


Figure 16. Electrode design configuration for MEMS vibrating ring gyroscope. (a) Outside placement, (b) inside placement, and (c) both inside and outside placement.

The portion of the vibrating ring with the electrode is considered as a parallel plate capacitor driving and sensing mechanism in the MEMS vibrating ring gyroscopes. The concept of moving parallel plate capacitors is most commonly employed for MEMS vibrating gyroscopes. The capacitors store charge “ Q ” when the voltage “ V ” is applied to their terminals. The stored charge between the two parallel plates can be expressed as $Q = CV$.

The two parallel plate capacitors for a portion of the vibrating ring structure with the electrode are shown in Figure 17. The capacitance “ C ” between the ring structures is given as Equation (40). Where y_o represents the gap between the two electrodes, w is the same width for both electrodes, h is the same height for both electrodes, and ϵ_o is the free-space permittivity constant.

$$C = \frac{\epsilon_o w h}{y_o} \tag{40}$$

The energy stored in the capacitor is usually found as a function of charge and by using Equation (41).

$$U_Q = \frac{1}{2} \frac{Q^2}{C} \tag{41}$$

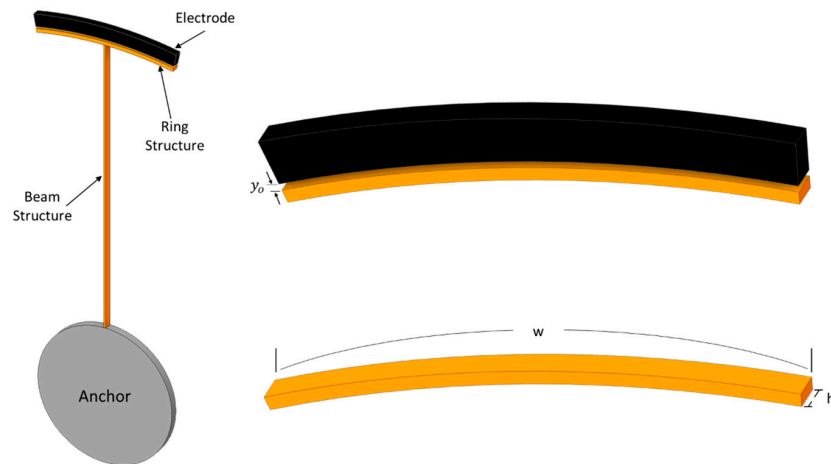


Figure 17. A schematic view of parallel plate capacitor for MEMS vibrating ring gyroscope.

In the same way, the energy stored in terms of voltage can be determined by using the above equation as the function of voltage.

$$U_V = \frac{1}{2}CV^2 \tag{42}$$

MEMS vibrating ring gyroscopes require actuation and detection mechanisms for their operations. The most popular and easy-to-implement method is electrostatic for actuation and capacitive for detection. Electrostatic actuation and capacitive detection offer many advantages over other methods as they provide good results and are easy to implement. This section will cover the electrostatic actuation and capacitive detection mechanisms for MEMS vibrating ring gyroscopes.

3.2. Basics of Electrostatic Actuation

Electrostatic actuation is a common mechanism to be utilized in the operation of MEMS vibrating gyroscopes. This mechanism generates electrostatic forces between the two closely placed electrodes. The generated electrostatic forces induce oscillations in the ring structure and maintain those oscillations for driving and sensing purposes. The parallel plate electrodes cause this electrostatic actuation. The electrostatic force field arises when the voltages are applied between the two parallel electrodes.

In the MEMS vibrating ring gyroscope, the electrostatic actuation force provides and regulates the ring structure’s continuous oscillation. The parallel plate electrodes generate the electrostatic force via actuation, creating a conservative force between the parallel electrodes. The voltage around the parallel plate electrodes is precisely controlled. The generated electrostatic force is expressed below.

$$F_e = \frac{\partial U_V}{\partial e} \tag{43}$$

$$F_e = \frac{1}{2} \frac{\partial C}{\partial e} V^2 = \frac{1}{2} \frac{\epsilon_0 w h V^2}{(y_0 - e)^2} \tag{44}$$

where F_e is the electrostatic force, $\epsilon_0 = 8.85 \times 10^{-12}$ Farads per meter (F/m) is the permittivity of free space, h is the height of the electrode, w is the width of the electrode, y_0 is the gap between the parallel electrodes, and e is the displacement of the ring that ultimately reduces the gap between the parallel plates. The schematic diagram of the two parallel plates is shown in Figure 18.

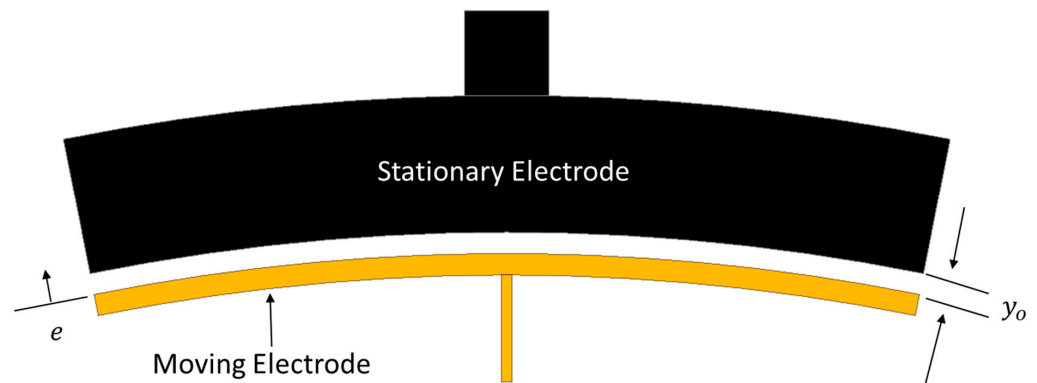


Figure 18. A schematic electrostatic actuation model for MEMS vibrating ring gyroscope.

MEMS Vibrating Ring Gyroscope Actuation

The ring structure in the MEMS vibrating ring gyroscope oscillates by an electrostatic actuation that is generated by applying a voltage across the parallel plate capacitors. The electrostatic actuation force generated by the set of electrodes is directly proportional to the square of the applied voltage difference. When a sinusoidal actuation force is needed, the actuation applied voltages must be selected appropriately to linearize the driving force. The total electrostatic force equation generated by the two opposite parallel plate capacitors C_1 and C_2 is given below.

$$F_t = \frac{1}{2} \frac{\partial C_1}{\partial e} V_1^2 - \frac{1}{2} \frac{\partial C_2}{\partial e} V_2^2 \tag{45}$$

The net balanced electrostatic actuation is a widely used strategy to compensate the force as linear with respect to the steady bias voltage V_{DC} and an alternating voltage v_{AC} . This technique involves applying a voltage $V_1 = V_{DC} + v_{AC}$ to one set of driving electrodes and a voltage $V_2 = V_{DC} - v_{AC}$ to the opposite set of driving electrodes, as presented schematically in Figure 19. In a symmetrical vibrating ring gyroscope, the overall electrostatic force simplifies to

$$F_b = 2 \frac{\partial C}{\partial e} V_{DC} v_{AC} \tag{46}$$

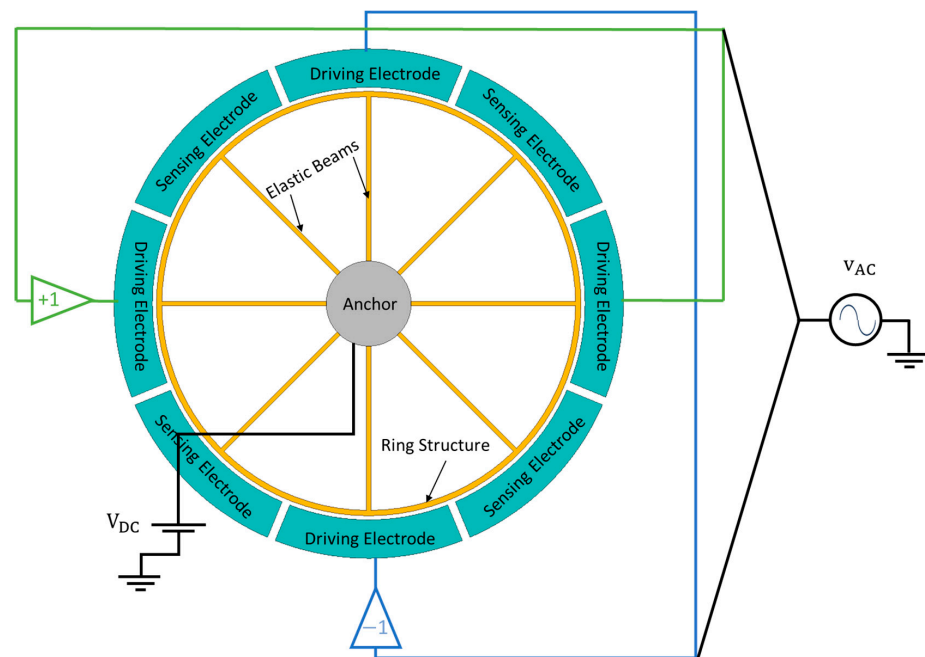


Figure 19. A schematic representation of the balanced electrostatic actuation method for the vibrating ring gyroscope.

The MEMS vibrating ring gyroscope’s electrostatic actuator structure can be determined using Equation (47).

$$F_{b-g} = 2 \frac{\epsilon_0 whN}{y_0^2} V_{DC} v_{AC} \tag{47}$$

where F_{b-g} is the net electrostatic actuation force for the MEMS vibrating ring gyroscope, N is the number of driving electrodes and ring portion, y_0 is the gap between the two electrodes, V_{DC} is the steady bias voltage, and v_{AC} is an alternating voltage.

3.3. Basics of Capacitive Detection

There are various methods to detect the deflection at sensing electrodes of the MEMS vibrating ring gyroscope. The capacitive detection method is quite popular and easy to design for gyroscopic operation. The capacitance of the parallel plate capacitors with a gap y_0 and overlap area A_0 is expressed as Equation (48).

$$C = \epsilon_0 \epsilon_r \frac{wh}{y_0} = \epsilon_0 \epsilon_r \frac{A_0}{y_0} \tag{48}$$

where ϵ_r is the dielectric value of the material between the parallel plate capacitors, and the deflection of the ring structure changes the gap y_0 between the electrodes. The microfabrication requirements usually determine the ring-to-electrode gap; this gap usually ranges from a few micrometers to a sub-micrometer value. Even a very small deflection provides a high capacitance value.

The capacitance is a nonlinear function of the deflection in capacitive detection for parallel plate capacitors. However, the change in capacitance can be linearized because the deflections used to be very small as compared to the gap between the two electrodes. Let us denote the deflection as d , which is assumed to be very small compared to the gap. The change in capacitance can be determined by using Equation (49).

$$\Delta C = \epsilon_0 \frac{wh}{y_0 - d} - \epsilon_0 \frac{wh}{y_0} \cong \epsilon_0 \frac{wh}{y_0^2} d \tag{49}$$

MEMS Vibrating Ring Gyroscope Differential Detection

The ring structure oscillates as an elliptical shape, and when the gyroscope is exposed to the external rotation, the same elliptical shape of deflection starts to appear on the sensing electrodes. The sensing electrodes sense the deflection as capacitive detection between two parallel plate electrodes. The deflection appears orthogonally on the sensing electrodes in the MEMS vibrating ring gyroscope design. The change in capacitance is detected on two orthogonal sets of electrodes. Differential capacitance detection is used to linearize the change in capacitance with deflections. The symmetrical sets of sensing electrodes are placed around the vibrating ring structure. The schematic diagram of the capacitive detection for the MEMS vibrating ring gyroscope is shown in Figure 20.

When the vibrating ring gyroscope oscillates in the sensing direction, the opposite sets of symmetrical electrodes sense the positive deflection along the sensing electrodes and the higher capacitance C_{D+} at those respective electrodes. At the same time, the elliptical ring is away from the other set of sensing electrodes; then, the lower capacitance C_{D-} value is detected on those electrodes. In this way, the differential detection method is expressed mathematically below.

$$C_{D+} = \epsilon_0 \frac{whN}{y_0 - d} \tag{50}$$

$$C_{D-} = \epsilon_0 \frac{whN}{y_0 + d} \tag{51}$$

$$\Delta C = C_{D+} - C_{D-} \cong 2\epsilon_0 \frac{whN}{y_0^2} d \tag{52}$$

In Equation (52), the change in capacitance is inversely proportional to the square of the gap between the two parallel plate electrodes. Therefore, it is believed to minimize the gap between the electrodes to enhance the sensitivity and performance of the vibrating ring gyroscopes.

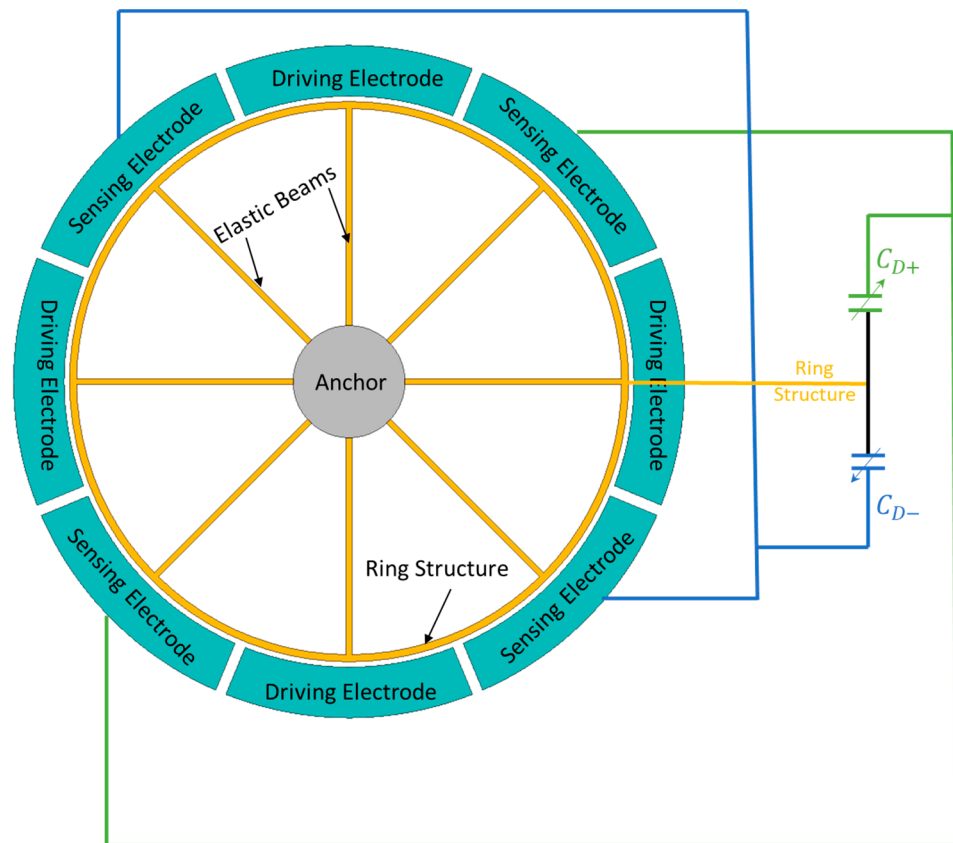


Figure 20. A schematic representation of the differential detection method for the vibrating ring gyroscope.

4. Damping Design

Damping in the MEMS vibrating gyroscopes means a decrease in the amplitude of the oscillations in the gyroscope operation over time. It is the energy that is being lost to the surroundings. In any oscillatory system like a gyroscope, damping is one of the important parameters to control the vibrations and stabilize the system. The following types of damping are discussed below for the MEMS vibrating ring gyroscope.

4.1. Viscous Damping

Vibrating structures are subject to viscous damping phenomena due to the resistance offered by the surrounding gases. The vibrating ring, stationary electrodes, and anchor placements cause the viscous damping in the MEMS vibrating ring gyroscope. Due to the drag force in the gyroscope’s stationary and oscillating systems, the motion of the ring structure through the atmosphere results in energy dissipation. Typically, viscous damping is linear and proportional to the vibrating ring structure’s velocity.

Squeeze film damping is a type of viscous damping. It occurs when two parallel plate surfaces move toward one another and compress the gas-filled space between them. The concept of squeeze film damping for the MEMS vibrating ring gyroscope is quite complex due to the energy dissipation and system stiffness effects. The effective viscosity is crucial

for describing the behavior of a gas or its rarefaction effects in squeeze film damping. The term effective viscosity v_e in squeeze film damping is given by [40].

$$v_e = \frac{v}{1 + 9.638 K_n^{1.159}} \tag{53}$$

where v is the actual velocity of the gas, and K_n is the Knudsen number, which defines the rarefaction effect and is dimensionless. The solution of the linearized Reynolds equation attributes one of the forces as inphase with the movement of the parallel plates, and the other force is outphase. Both inphase and outphase forces are spring F_{sf} and damping forces F_{sk} , respectively. The equations for the respective forces are given by [41], which are shown below.

$$\frac{F_{sf}}{y} = \frac{64\sigma P_a A}{\pi^6 d} \sum_{m,n \text{ odd}} \frac{m^2 + c^2 n^2}{(mn)^2 \left[(m^2 + c^2 n^2)^2 + \frac{\sigma^2}{\pi^4} \right]} \tag{54}$$

$$\frac{F_{sk}}{y} = \frac{64\sigma P_a A}{\pi^8 d} \sum_{m,n \text{ odd}} \frac{m^2 + c^2 n^2}{(mn)^2 \left[(m^2 + c^2 n^2)^2 + \frac{\sigma^2}{\pi^4} \right]} \tag{55}$$

where y is the deflection of the plate, d is the spacing between the plates, m and n are odd integers, $A = w h$ is the area of the parallel plate, $c = h/w$, h is the height, w is the length of the plate, and P_a is the ambient pressure. The squeeze number σ is given by [42]. Where ω is the angular frequency.

$$\sigma = \frac{12v_e h^2}{P_a d^2} \omega \tag{56}$$

4.2. Structural Damping

Structural damping for the MEMS vibrating gyroscope depends on the material’s internal structure. This kind of damping is quite a complex model. An easy method is to describe first the material’s properties and then proceed to the damping properties. The model could be analyzed using finite element method Ansys 2023 R1.

$$F_{sd} = -\tau \omega y \tag{57}$$

where F_{sd} is the structural damping force, τ is the loss parameter related to the material’s internal friction, ω is the frequency, y is the deflection of the vibrating element.

4.3. Thermoelastic Damping

Thermoelastic damping is one of the main damping mechanisms under vacuum conditions. It is a phenomenon of the material’s intrinsic behavior in which the system dissipates thermal energy because of the elastic deformation in the system. In the vibrating ring structure, the tensile and compressive forces generate heat dissipation in the vibrating system that finally affects the vibrational energy of the system. Thermoelastic damping significantly affects the gyroscope quality factor under vacuum conditions ranging from 100 k to 200 k values. The thermoelastic loss factor τ_{TED} can be determined by the given Equation (58).

$$\tau_{TED} = \frac{\alpha^2 G}{\rho C_p V} \int \left(\frac{\partial \sigma}{\partial T} \right)^2 dV \tag{58}$$

where α is the coefficient of thermal expansion, G is the shear modulus of the material, ρ is the density of the material, C_p is the specific heat at constant pressure, V is the volume, σ is the stress, and T is the operating temperature of the vibrating system.

4.4. Anchor Damping

Anchor damping could be determined by modeling with consideration of the energy losses at the anchor points through the anchor’s design and material properties. This type

of damping can be predicted through an accurate finite element analysis. The following simple equation could be used for evaluating anchor damping.

$$F_{ad} = -\tau_a y \quad (59)$$

where F_{ad} is the damping force, τ_a is the anchor loss factor, and y is the deflection of the vibrating structure in the MEMS vibrating gyroscope.

5. Microfabrication

The MEMS vibrating ring gyroscopes' operation depends on the microscale vibrating structures. In recent years, the technological revolution in microfabrication processes has allowed technology to fabricate microscale intricate MEMS designs for various applications. The micromachining process in the MEMS fabrication originated from the semiconductor fabrication processes. The micromachining process enables the merging of the microscale mechanical and electrical components on the same electronic chip to operate on the respective MEMS devices.

In recent developments, many microfabrication processes have been introduced to fabricate various free-standing microscale vibrating structures on the wafers. The microfabrication process of the vibrating ring gyroscopes involves many complex steps. The gyroscope design structure is usually patterned layer by layer by different microfabrication techniques. Each layer is designed for distinguishing purposes. Silicon on insulator (SOI) is a technique of bulk micromachining that is currently quite popular in the fabrication of MEMS vibrating ring gyroscopes. The section below highlights the SOI process for the MEMS vibrating ring gyroscope.

5.1. Silicon on Insulator

Silicon on insulator (SOI) wafers provide base material for the bulk micromachining process. The structural layer of silicon material is bonded on the insulator layer. The structural layer patterned above on the oxide layer makes them electrically isolated with the mechanically supported free-standing structures. The SOI wafers with varied layer thicknesses of structural, oxide, and others with varying conductivities fulfill the complex design requirements for the MEMS vibrating ring gyroscopes.

The basic, simple, and quite cheap SOI microfabrication process was introduced by the Multi-User MEMS Processes (SOIMUMPs) [43]. There is no substrate placed under the structural layer in this process, which ultimately provides high-aspect-ratio structures with low air damping. These two characteristics are essential to design the high-performance MEMS vibrating ring gyroscope. SOI is a single-wafer microfabrication process that allows for patterning and etching on the wafer with various thicknesses of the four mask layers. The process can offer specific thicknesses of the structural layer, and the minimum feature size in μm .

5.2. Post-Fabrication Process

The post-fabrication process includes various steps, from dicing the gyroscopes to placement in the dual inline package (DIP) for static to dynamic characterizations. A schematic illustration of the MEMS vibrating ring gyroscope after the microfabrication processes is shown in Figure 21. A complete design of the vibrating ring gyroscope is placed into the DIP, where the gyroscope's electrodes are connected to the electrical pads in DIP with the wire bonding process for the MEMS device characterizations.

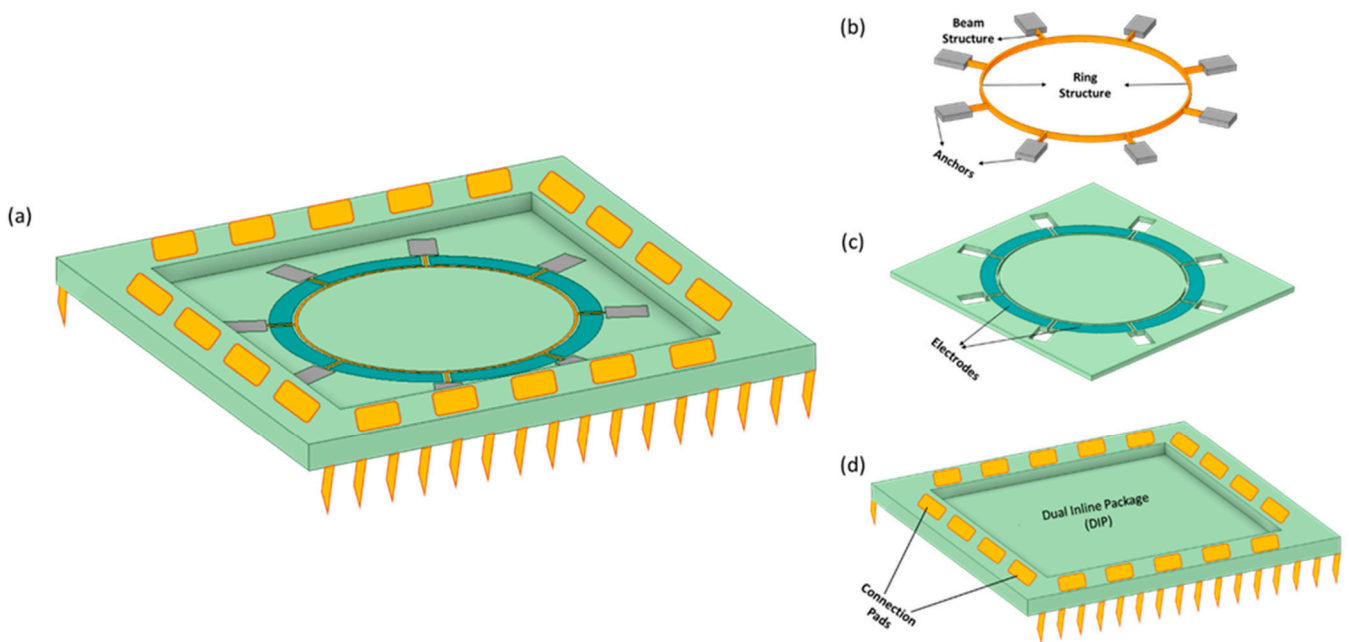


Figure 21. A schematic illustration of a complete MEMS vibrating ring gyroscope placed into the package (a) Complete design kit for characterization (b) Vibrating Ring Gyroscope (c) Electrodes and Support Structure (d) DIP.

5.3. Material Selection

The selection of material is essential for fabricating the MEMS vibrating ring gyroscope. The material properties significantly impact the mode mismatch frequencies and the quality factor of the gyroscope. Silicon is the primary material for the MEMS vibrating ring gyroscope because of its high availability, low fabrication, and low overall costs. Different forms of silicon material have been extensively used in the fabrication of MEMS vibrating ring gyroscopes, some of which are listed below.

Single Crystal Silicon (SCS): It is one of the most commonly used materials in the fabrication of MEMS devices. The SCS has two primary orientations (100) and (111) [44]. Each orientation possesses different properties that can be advantageous or disadvantageous in terms of the fabrication of the MEMS devices. A (100) SCS is highly anisotropic, resulting in a MEMS vibrating ring gyroscope that tends to have a higher mode mismatch between driving and sensing resonance frequencies. Anisotropy indicates that the mechanical properties of a material can vary depending on the direction. The different directions of (100) silicon possess different Young’s modulus and Poisson ratio values that react differently when exposed to the etching process and subsequently undercut the defined structures. The faster etching rate of (100) SCS, which can reduce the fabrication time, is a significant advantage of its use. However, there is a disadvantage regarding the high number of mode mismatch resonance frequencies. However, due to the symmetric structure of the ring, the mode mismatch can be reduced by adjusting the width and placement of the beams regarding the gyroscope anchor’s design. The anchor design can accommodate the various placement shifts of the beams, and this can be done by exhaustive parametric modeling of the design parameters.

Polysilicon: Another material extensively utilized for MEMS vibrating ring gyroscope fabrication. Polysilicon MEMS vibrating ring gyroscopes typically have a low-quality factor. A low-quality factor results in more significant energy loss, which may compromise the gyroscope’s sensitivity and precision.

Fused Silica: It is distinguished by its isotropic properties, in which its properties are the same in all directions. In addition to its low thermoelastic damping and better temperature stability, it is a quite suitable material for gyroscope fabrication for harsh environments. The vibrating ring gyroscopes that comprise fused silica provide excel-

lent gyroscope performance. However, MEMS fabrication techniques are not completely compatible with fused silica as the material for vibrating gyroscopes.

The material selection for MEMS vibrating ring gyroscopes is an important parameter. Each material has advantages and disadvantages, and ongoing research seeks to optimize these properties for improved gyroscope performance.

5.4. Imperfections in Vibrating Ring Gyroscope

The imperfections are always present in the MEMS vibrating ring gyroscope. These imperfections exist for many reasons, including fabrication and exposure to different environments. These imperfections cause frequency mode mismatches to reduce mechanical sensitivity, drifting, and noise in the gyroscope operations. Some of them are discussed below.

5.4.1. Microfabrication Imperfections

The anisotropy of material and microfabrication imperfections could not be completely mitigated from the overall process. The microfabrication errors affect the material characteristics and design of the MEMS structures. The structures' thickness depends on the deposition rate and processes, and the width of the structure elements depends on the etching processes. The non-uniformity of the etching processes causes the mechanical structures' undercuts, often called side wall angles. These anomalies affect the resonance frequencies of the vibrating ring gyroscope, resulting in mode mismatching. The mode mismatch significantly deteriorates the performance of the gyroscope. The equation below can be used to find the mode mismatch because of the imperfections of microfabrication.

$$\Delta f = f_s - f_d = \frac{1}{2\pi}(\omega_s - \omega_d) \quad (60)$$

where ω_s and ω_d are the sense mode and drive mode frequency of the system. The deposition process alters the Young's modulus of the material, and undercuts, fluctuations in the damping parameters, and other related factors significantly affect the performance of the gyroscope.

These errors can be minimized by analyzing the prefabrication design study prior to the fabrication of the MEMS vibrating ring gyroscope. The symmetric design of the ring gyroscope provides better results as the design has the same configurations in the other directions, which impacts the gyroscope overall. For example, material anisotropy can be minimized by adjusting the location of the beam structures connected to the anchors. However, these adjustments require extensive design parametric modeling to mitigate the effects of the imperfections of the fabrications.

Prefabrication Design Modification: This design approach requires extensive parametric modeling of various design parameters. In a vibrating ring gyroscope, the widths of the beam structures and ring structure can be modeled in accordance with microfabrication undercuts because of different etching rates. A comparative design parameters analysis was performed to minimize the mode mismatch for the vibrating ring gyroscope for silicon (100) [6]. There is another method to increase or decrease the ring's mass to gain the optimal results in vibrating ring gyroscopes. This method was successfully demonstrated [45] by tailoring the mass of the rings to eliminate the mode mismatch from 15 Hz to less than 100 mHz for 14 kHz gyroscope resonance frequencies.

Tuning Frequencies: The other design approach mitigates the errors by adjusting and matching the resonance frequencies. The design structure of the vibrating ring gyroscope provides enough space to accommodate as many electrodes as possible around the ring structure. As described in the electrical design section, these electrodes could be used for multiple purposes such as tuning and quadrature electrodes. This method can reduce the gap between the two operating resonance frequencies [46]. This method uses the electrostatic stiffness effect and adjusts the mode mismatch. In other words, the driving resonance frequency is adjusted in a way to equal the sensing resonance frequency, as

shown in Equation (60) ($\omega_d = \omega_s$), so the mode mismatch becomes zero. This tuning frequency approach is used to maximize the mechanical sensitivity of the vibrating ring gyroscope.

5.4.2. Temperature Effects

A vibrating ring gyroscope generally faces difficulty maintaining the scale factor's stability and bias when exposed to various temperature profiles. Temperature differences in MEMS gyroscopes proceed to thermal expansion, ultimately affecting the gyroscope design geometry and the actuation and detection electrodes. Also, due to temperature changes, these thermal expansions and contractions can introduce stresses in the MEMS structure, further affecting the stiffness of the MEMS gyroscope. The temperature fluctuations affect the design geometry of the gyroscope, which affects the Young's modulus of the material, impacting the stiffness of the structure. Furthermore, the temperature fluctuations affect the gyroscope's scale factor and bias.

Due to their symmetric design structure, MEMS vibrating ring gyroscopes usually have uniform thermal expansion into the ring geometry [29]. The vibrating ring gyroscope generally operates at two identical elliptical modes of vibrations. Therefore, the uniform temperature effect affects both modes with the same thermal expansion. Therefore, the vibrating ring designs have the same expansion in the whole geometry, making them quite suitable and robust against temperature fluctuations.

6. Conclusions

This paper presents an exhaustive analysis of the MEMS vibrating ring gyroscopes, exploring the complexities of mechanical, electrical, damping, material, and microfabrication design considerations. A number of different setups of electrode designs, beam structures designs, and frame designs are studied; each design finding presents its own set of difficulties and opportunities in the MEMS gyroscope field. The paper further investigates the effects of various types of damping, including viscous, structural, thermoelastic, and anchor damping, and their roles on the performance of the vibrating ring gyroscope. The complexities of the microfabrication processes are pivotal in developing the MEMS vibrating ring gyroscopes, including the effects of material selection to the effects of temperature variations. These findings contribute to a better understanding of the MEMS vibrating ring gyroscope technology and make avenues for further future investigations in fields such as navigation systems and other related electronics applications. The research analysis between design complexity, performance, and size limitations is an important objective, highlighting the complexity of MEMS vibrating ring gyroscope design.

Author Contributions: The conceptualization was given by K.M. and I.H. All the designing, finding, and preparation of the figures was carried out by W.A.G. Writing: Review and editing of the final draft were performed by W.A.G. Supervision was performed by I.H., I.M. and K.M. All authors have read and agreed to the published version of the manuscript.

Funding: This research was funded through research support program by research training program (RTP) of the Australian government through Curtin University.

Data Availability Statement: Not applicable.

Conflicts of Interest: The authors declare no conflict of interest.

References

1. Shaeffer, D.K. MEMS inertial sensors: A tutorial overview. *IEEE Commun. Mag.* **2013**, *51*, 100–109. [[CrossRef](#)]
2. Acar, C.; Schofield, A.R.; Trusov, A.A.; Costlow, L.E.; Shkel, A.M. Environmentally robust MEMS vibratory gyroscopes for automotive applications. *IEEE Sen. J.* **2009**, *9*, 1895–1906. [[CrossRef](#)]
3. Ren, X.; Zhou, X.; Yu, S.; Wu, X.; Xiao, D. Frequency-modulated mems gyroscopes: A review. *IEEE Sen. J.* **2021**, *21*, 26426–26446. [[CrossRef](#)]
4. Xia, D.; Yu, C.; Kong, L. The development of micromachined gyroscope structure and circuitry technology. *Sensors* **2014**, *14*, 1394–1473. [[CrossRef](#)]

5. Liu, K.; Zhang, W.; Chen, W.; Li, K.; Dai, F.; Cui, F.; Wu, X.; Ma, G.; Xiao, Q. The development of micro-gyroscope technology. *J. Micromech. Microeng.* **2009**, *19*, 113001. [[CrossRef](#)]
6. Hyun An, B.; Gill, W.A.; Lee, J.S.; Han, S.; Chang, H.K.; Chatterjee, A.N.; Choi, D.S. Micro-electromechanical vibrating ring gyroscope with structural mode-matching in (100) silicon. *Sens. Lett.* **2018**, *16*, 548–551. [[CrossRef](#)]
7. Jia, J.; Ding, X.; Qin, Z.; Ruan, Z.; Li, W.; Liu, X.; Li, H. Overview and analysis of MEMS Coriolis vibratory ring gyroscope. *Measurement* **2021**, *182*, 109704. [[CrossRef](#)]
8. Yoon, S.W.; Lee, S.; Najafi, K. Vibration sensitivity analysis of MEMS vibratory ring gyroscopes. *Sens. Actuators A Phys.* **2011**, *171*, 163–177. [[CrossRef](#)]
9. Gallacher, B.J. Principles of a micro-rate integrating ring gyroscope. *IEEE Trans. Aerosp. Electron. Syst.* **2012**, *48*, 658–672. [[CrossRef](#)]
10. Gill, W.A.; Ali, D.; An, B.H.; Syed, W.U.; Saeed, N.; Al-shaibah, M.; Elfadel, I.M.; Al Dahmani, S.; Choi, D.S. MEMS multi-vibrating ring gyroscope for space applications. *Microsyst. Technol.* **2020**, *26*, 2527–2533. [[CrossRef](#)]
11. Ayazi, F.; Najafi, K. A HARPSS polysilicon vibrating ring gyroscope. *J. Microelectromech. Syst.* **2001**, *10*, 169–179. [[CrossRef](#)]
12. Cao, H.; Liu, Y.; Kou, Z.; Zhang, Y.; Shao, X.; Gao, J.; Huang, K.; Shi, Y.; Tang, J.; Shen, C. Design, fabrication and experiment of double U-beam MEMS vibration ring gyroscope. *Micromachines* **2019**, *10*, 186. [[CrossRef](#)] [[PubMed](#)]
13. Ayazi, F.; Najafi, K. Design and fabrication of high-performance polysilicon vibrating ring gyroscope. In Proceedings of the Proceedings MEMS 98. IEEE. Eleventh Annual International Workshop on Micro Electro Mechanical Systems. An Investigation of Micro Structures, Sensors, Actuators, Machines and Systems (Cat. No. 98CH36176), Heidelberg, Germany, 25–29 January 1998; pp. 621–626.
14. Kou, Z.; Liu, J.; Cao, H.; Shi, Y.; Ren, J.; Zhang, Y. A novel MEMS S-springs vibrating ring gyroscope with atmosphere package. *AIP Adv.* **2017**, *7*, 125301. [[CrossRef](#)]
15. Syed, W.U.; An, B.H.; Gill, W.A.; Saeed, N.; Al-Shaibah, M.; Al Dahmani, S.; Choi, D.; Elfadel, I.A.M. Sensor Design Migration: The Case of a VRG. *IEEE Sen. J.* **2019**, *19*, 10336–10346. [[CrossRef](#)]
16. Gill, W.A.; Howard, I.; Mazhar, I.; McKee, K. MEMS Vibrating Ring Gyroscope with Worm-Shaped Support Springs for Space Applications. *Eng. Proc.* **2022**, *31*, 2.
17. Senkal, D.; Askari, S.; Ahamed, M.; Ng, E.; Hong, V.; Yang, Y.; Ahn, C.H.; Kenny, T.; Shkel, A. 100K Q-factor toroidal ring gyroscope implemented in wafer-level epitaxial silicon encapsulation process. In Proceedings of the 2014 IEEE 27th International Conference on Micro Electro Mechanical Systems (MEMS), San Francisco, CA, USA, 26–30 January 2014; pp. 24–27.
18. Challoner, A.D.; Howard, H.G.; Liu, J.Y. Boeing disc resonator gyroscope. In Proceedings of the 2014 IEEE/ION Position, Location and Navigation Symposium-PLANS 2014, Monterey, CA, USA, 5–8 May 2014; pp. 504–514.
19. Su, T.-H.; Nitzan, S.H.; Taheri-Tehrani, P.; Kline, M.H.; Boser, B.E.; Horsley, D.A. Silicon MEMS disk resonator gyroscope with an integrated CMOS analog front-end. *IEEE Sen. J.* **2014**, *14*, 3426–3432. [[CrossRef](#)]
20. Xu, Y.; Li, Q.; Wang, P.; Zhang, Y.; Zhou, X.; Yu, L.; Wu, X.; Xiao, D. 0.015 degree-per-hour honeycomb disk resonator gyroscope. *IEEE Sen. J.* **2020**, *21*, 7326–7338. [[CrossRef](#)]
21. Zaman, M.F.; Sharma, A.; Ayazi, F. The resonating star gyroscope: A novel multiple-shell silicon gyroscope with sub-5 deg/hr allan deviation bias instability. *IEEE Sen. J.* **2009**, *9*, 616–624. [[CrossRef](#)]
22. Chen, F.; Wen, Z.; Xu, D.; Zhou, W.; Li, X. An Anti-Aliasing and Self-Clocking $\Sigma\Delta$ Cobweb-Like Disk Resonant MEMS Gyroscope with Extended Input Range. In Proceedings of the 2021 IEEE 34th International Conference on Micro Electro Mechanical Systems (MEMS), Virtual, 25–29 January 2021; pp. 334–337.
23. Fan, B.; Guo, S.; Cheng, M.; Yu, L.; Zhou, M.; Hu, W.; Zheng, F.; Bu, F.; Xu, D. Frequency symmetry comparison of cobweb-like disk resonator gyroscope with ring-like disk resonator gyroscope. *IEEE Electron Device Lett.* **2019**, *40*, 1515–1518. [[CrossRef](#)]
24. Wu, X.; Xi, X.; Wu, Y.; Xiao, D. *Cylindrical Vibratory Gyroscope*; Springer: Berlin/Heidelberg, Germany, 2021.
25. Basarab, M.; Lunin, B.; Matveev, V.; Chumankin, E. Static balancing of metal resonators of cylindrical resonator gyroscopes. *Gyroscopy Navig.* **2014**, *5*, 213–218. [[CrossRef](#)]
26. Lee, J.S.; An, B.H.; Mansouri, M.; Yassi, H.A.; Taha, I.; Gill, W.A.; Choi, D.S. MEMS vibrating wheel on gimbal gyroscope with high scale factor. *Microsyst. Technol.* **2019**, *25*, 4645–4650. [[CrossRef](#)]
27. Gill, W.A.; Howard, I.; Mazhar, I.; McKee, K. A review of MEMS vibrating gyroscopes and their reliability issues in harsh environments. *Sensors* **2022**, *22*, 7405. [[CrossRef](#)] [[PubMed](#)]
28. Khan, I.; Ting, D.S.; Ahamed, M.J. Design and development of a MEMS vibrating ring resonator with inner rose petal spring supports. *Microsyst. Technol.* **2021**, *27*, 985–995. [[CrossRef](#)]
29. He, G.; Najafi, K. A single-crystal silicon vibrating ring gyroscope. In Proceedings of the Technical Digest. MEMS 2002 IEEE International Conference. Fifteenth IEEE International Conference on Micro Electro Mechanical Systems (Cat. No. 02CH37266), Las Vegas, NV, USA, 24 January 2002; pp. 718–721.
30. Shkel, A.M.; Horowitz, R.; Seshia, A.A.; Park, S.; Howe, R.T. Dynamics and control of micromachined gyroscopes. In Proceedings of the 1999 American Control Conference (Cat. No. 99CH36251), San Diego, CA, USA, 2–4 June 1999; pp. 2119–2124.
31. Hosseini-Pishrobat, M.; Tatar, E. Analysis of quadrature and frequency split in a MEMS vibrating ring gyroscope with structural imperfections. In Proceedings of the 2021 21st International Conference on Solid-State Sensors, Actuators and Microsystems (Transducers), Orlando, FL, USA, 20–24 June 2021; pp. 1291–1294.

32. Qin, Z.; Gao, Y.; Jia, J.; Ding, X.; Huang, L.; Li, H. The effect of the anisotropy of single crystal silicon on the frequency split of vibrating ring gyroscopes. *Micromachines* **2019**, *10*, 126. [[CrossRef](#)] [[PubMed](#)]
33. Acar, C.; Shkel, A. Mechanical design of MEMS gyroscopes. In *MEMS Vibratory Gyroscopes: Structural Approaches to Improve Robustness*; Springer: Berlin/Heidelberg, Germany, 2009; pp. 1–38.
34. Acar, C.; Shkel, A. *MEMS Vibratory Gyroscopes: Structural Approaches to Improve Robustness*; Springer Science & Business Media: Berlin/Heidelberg, Germany, 2008.
35. Hearn, E.J. *Mechanics of Materials 2: The Mechanics of Elastic and Plastic Deformation of Solids and Structural Materials*; Elsevier: Amsterdam, The Netherlands, 1997.
36. Hagedorn, P.; DasGupta, A. *Vibrations and Waves in Continuous Mechanical Systems*; John Wiley & Sons: Hoboken, NJ, USA, 2007.
37. Gill, W.A.; Howard, I.; Mazhar, I.; McKee, K. Development of Starfish-Shaped Two-Ring Microelectromechanical Systems (MEMS) Vibratory Ring Gyroscope with C-Shaped Springs for Higher Sensitivity. *Eng. Proc.* **2022**, *27*, 36.
38. Putty, M.W. *A Micromachined Vibrating Ring Gyroscope*; University of Michigan: Ann Arbor, MI, USA, 1995.
39. Xiao, D.; Yu, D.; Zhou, X.; Hou, Z.; He, H.; Wu, X. Frequency tuning of a disk resonator gyroscope via stiffness perturbation. *IEEE Sen. J.* **2017**, *17*, 4725–4734. [[CrossRef](#)]
40. Veijola, T.; Kuisma, H.; Lahdenperä, J.; Ryhänen, T. Equivalent-circuit model of the squeezed gas film in a silicon accelerometer. *Sens. Actuators A Phys.* **1995**, *48*, 239–248. [[CrossRef](#)]
41. Blech, J.J. On isothermal squeeze films. *J. Tribol.* **1983**, *105*, 615. [[CrossRef](#)]
42. Griffin, W.S.; Richardson, H.H.; Yamanami, S. A study of fluid squeeze-film damping. *J. Basic Eng.* **1966**, *88*, 451–456. [[CrossRef](#)]
43. Cowen, A.; Hames, G.; Monk, D.; Wilcenski, S.; Hardy, B. *SOIMUMPs Design Handbook*; Memscap Inc.: Durham, NC, USA, 2011; pp. 2002–2011.
44. Hopcroft, M.A.; Nix, W.D.; Kenny, T.W. What is the Young’s Modulus of Silicon? *J. Microelectromech. Syst.* **2010**, *19*, 229–238. [[CrossRef](#)]
45. Behbahani, A.H.; Kim, D.; Stupar, P.; DeNatale, J.; M’Closkey, R.T. Tailored etch profiles for wafer-level frequency tuning of axisymmetric resonators. *J. Microelectromech. Syst.* **2017**, *26*, 333–343. [[CrossRef](#)]
46. Gallacher, B.J.; Hedley, J.; Burdess, J.S.; Harris, A.J.; Rickard, A.; King, D.O. Electrostatic correction of structural imperfections present in a microring gyroscope. *J. Microelectromech. Syst.* **2005**, *14*, 221–234. [[CrossRef](#)]

Disclaimer/Publisher’s Note: The statements, opinions and data contained in all publications are solely those of the individual author(s) and contributor(s) and not of MDPI and/or the editor(s). MDPI and/or the editor(s) disclaim responsibility for any injury to people or property resulting from any ideas, methods, instructions or products referred to in the content.